Available online at www.sciencedirect.com
ScienceDirect
Journal of Hazardous Materials 156 (2008) 178–185
Journal of Hazardous Materials
www.elsevier.com/locate/jhazmat

Removal of arsenic from water using granular ferric hydroxide: Macroscopic and microscopic studies

Xiao-Hong Guan [a,b,c], Jianmin Wang [b,c,*], Charles C. Chusuei [d]

[a] School of Municipal and Environmental Engineering, Harbin Institute of Technology, Harbin, PR China
[b] Department of Civil, Architectural & Environmental Engineering, Missouri University of Science and Technology, 1870 Miner Circle, Rolla, MO 65409, USA
[c] Environmental Research Center (ERC) for Emerging Contaminants, Missouri University of Science and Technology, 1870 Miner Circle, Rolla, MO 65409, USA
[d] Department of Chemistry, Missouri University of Science and Technology, 1870 Miner Circle, Rolla, MO 65409, USA

Received 27 September 2007; received in revised form 28 November 2007; accepted 4 December 2007
Available online 14 December 2007

Abstract

Removal of arsenate from water using granular ferric hydroxide (GFH) was investigated under different pH and As(V) loading conditions, using batch equilibrium adsorption, FTIR, and EXAFS methods. The arsenate adsorption envelopes on GFH exhibited broad adsorption maxima when the initial As(V) concentration was less than 500 mg/L at sorbent concentration of 10 g/L. As the initial As(V) concentration increased to 500, 1000 or 2000 mg/L for the same sorbent concentration, distinct adsorption maxima appeared and shifted to lower pH. Acidimetric–alkalimetric titration and arsenic adsorption isotherm data indicated that the surface of GFH is high heterogeneous. FTIR spectra revealed that complexes of two different structures, bidentate and monodentate, were formed upon the adsorption of arsenate on GFH, and bidentate complexes were only observed at pH values greater than 6. The EXAFS analyses confirmed that arsenate form bidentate binuclear complexes with GFH at pH 7.4 as evidenced by an average Fe-As(V) bond distance of 3.32 Å.
© 2008 Elsevier B.V. All rights reserved.

Keywords: Arsenic; Granular ferric hydroxide; Adsorption; FTIR; EXAFS

1. Introduction

Arsenic (As) is a toxic element occurring in natural waters in a variety of forms including soluble, particulate, and organic bound, but mainly as inorganic trivalent As(III) and pentavalent As(V) oxidation states. In recent years, arsenic contamination of water has become a major concern on a global scale [1]. The most common and serious route of arsenic exposure for humans is through the ingestion of drinking water containing arsenic compounds. Several areas of the world have relatively high arsenic concentrations in their groundwater used for drinking water. These areas include Taiwan (1.82 mg/L), Hungary (0.1 mg/L), India (0.05 mg/L), Mexico (0.4 mg/L), and the southwest United States (0.1 mg/L) [2]. Since arsenic is highly toxic and carcinogenic, the World Health Organization (WHO) has revised the guideline for arsenic in drinking water from 50 to 10 μg/L [3]. The U.S. environmental protection agency (USEPA) has adopted an arsenic maximum contaminant level (MCL) of 10 μg/L, which has been enforced since 23 January 2006 [4]. USEPA estimates that 3000 community water systems (CWS) and 1100 non-transient, non-community water systems will need to take measures to lower arsenic in drinking water.

The most commonly used removal techniques for arsenic from aqueous matrixes are (1) precipitation/coagulation processes using metal salts such as those of iron and aluminum; (2) precipitation/adsorption processes on activated alumina and oxides/hydroxides of mainly iron, but also manganese or lanthanum; (3) ion-exchange; (4) desalting techniques such as reverse osmosis or electrodialysis [5–7]. In the natural environment, As(V) strongly adsorbs to several common mineral surfaces, such as goethite, ferrihydrite, and alumina in soils and sediments [8,9]. Activated alumina, granular ferric hydroxide

* Corresponding author at: Department of Civil, Architectural & Environmental Engineering, University of Missouri-Rolla, 1870 Miner Circle, Rolla, MO 65409, USA. Tel.: +1 573 341 7503; fax: +1 573 341 4729.
E-mail address: wangjia@mst.edu (J. Wang).

0304-3894/$ – see front matter © 2008 Elsevier B.V. All rights reserved.
doi:10.1016/j.jhazmat.2007.12.012

(GFH), and ferric oxide adsorbents are widely used in the filtration treatment of arsenic [10–12]. Understanding the interactions between arsenic and metal (hydr)oxides, especially at high loadings, will enable the accurate description of arsenic mobility in the environment and the prediction of adsorptive properties of the adsorbents.

The pH was found to be a very important factor affecting arsenic removal. Some researchers found that almost 100% of arsenate was adsorbed at pH below a certain value while arsenate adsorption decreased considerably with further increase in pH [13–17]. Most of the researchers studied the adsorption envelopes at low adsorption densities and within a narrow pH range. However, the mechanisms of arsenate adsorption on minerals at high arsenic loading conditions, e.g. 10^3–10^4 mg/kg, have not previously been delineated. In practical applications using columns to remove arsenic, the equilibrium concentration of arsenic ranges from low (at the effluent end of the column) to high (equal to the influent concentration at the influent end of the column). In order to create a scenario that mimic the adsorption at the influent end of the column using batch systems, we need to use a high initial arsenic loading or concentration that results in the equilibrium concentration equivalent to the influent arsenic concentration.

A molecular-level understanding of the adsorption of arsenic by metal oxides and oxyhydroxides is needed to predict the long-term fate of arsenic in aqueous sediments. Previous spectroscopic studies [18–22], pressure-jump relaxation kinetics measurements [23,24] and titration measurements [25] showed that arsenate adsorbs to iron hydroxides by forming inner-sphere surface complexes through ligand exchange with hydroxyl groups at the mineral surface. However, there have been conflicting reports on the precise structure of the arsenate–iron hydroxide complex. Several structures have been postulated, including monodentate, bidentate binuclear and bidentate mononuclear complexes. Fendorf et al. [22] observed that at low arsenate surface coverages on goethite, monodentate complexation was favored while at higher coverage the bidentate complexes were more prevalent, in which the bidentate–binuclear complex appeared to be in the greatest proportion at the highest surface coverage. On the other hand, Waychunas et al. [18] showed that arsenate adsorption on ferrihydrite occurred predominantly as a bidentate binuclear complex and that monodentate surface complexation occurred to only a limited extent. The objective of the present study is to delineate the mode(s) of arsenate adsorption on GFH using adsorption envelope, FTIR and EXAFS analyses, under controlled pH and arsenic loading conditions to better understand how these variables govern binding between the arsenate and GFH surface.

2. Materials and methods

2.1. Chemicals and reagents

Reagent-grade chemicals and de-ionized (DI) water were used to prepare all solutions used in this study. Commercial GFH (GFH^{TM} media) was purchased from US Filter, Inc. and used as received.

2.2. GFH characterization

Electrophoretic mobility was used to determine the surface electrical characteristics of GFH particles at various pH values. GFH particles were diluted in 100 mL of 0.01 mol/L $NaNO_3$ solution. The pH of the solution was adjusted either by 0.1 mol/L NaOH or HNO_3 solution. The electrophoretic mobility was observed at room temperature with a Zetasizer 3000HSA (Malvern Instruments Ltd., UK). Morphological analysis of the GFH was performed by scanning electron microscopy (SEM) using a Hitachi S-570 LaB6 microscope (at 10 kV) (Hitachi Ltd., Tokyo, Japan). X-ray diffraction patterns of GFH were obtained by a Rigaku Miniflex diffractometer (Rigaku Americas, TX, USA) using the Cu Kα line at 1.542 Å operated at 40 kV and a current of 35 mA. Data were obtained over the range of 2θ from 0.3° to 60°. The BET specific surface area, pore volume and pore size distribution of GFH were examined with a Quantachrome Autosorb-1-C high performance surface area and pore size analyzer (Quantachrome Instruments, FL, USA). GFH was freeze-dried before it was subjected to characterization.

A batch equilibrium titration method was employed to determine the surface acid characteristics of GFH. The titration procedure was consisted of (a) distributing 1 g of GFH and 100 mL of DI water containing 0.1 mol/L $NaNO_3$ to each of a series of 125 mL bottles and recording the initial pH of the suspension; (b) adding different amounts of standard acid or base stock solution to these bottles to adjust the pH to the range of 1–13 (the volume of acid or base should be less than 5 mL for each case); no acid or base was added to one bottle (control unit); (c) shaking the bottles at 180 oscillation/min using a EBERBACH 6010 shaker for 24 h; (d) measuring the final pH, plot the acid/base addition volume as a function of pH to obtain an overall titration curve; (e) filtrating the suspensions and titrating the filtrate back to the pH of the control unit to get the back-titration curve; (f) developing a net titration curve by subtracting the acid/base consumed by the filtrate from the overall titration curve under the same pH condition.

2.3. As(V) adsorption experiments

Batch equilibrium adsorption experiments were conducted at 15 different pH values, ranging from pH 1 to 13 at initial arsenic concentrations in the range of 5–2000 mg/L. A broad arsenic concentration range was selected to evaluate the adsorption behavior of arsenate in different regions of the sorption isotherm: (i) the initial proportional adsorption region, (ii) the intermediate region, and (iii) the maximum adsorption region to simulate realistic conditions. The arsenic content of residual sludges from arsenic removal systems can be in the range of 10^3–10^4 mg/kg [11,26]. Thus, for a batch system with a sorbent concentration of 10 g/L, the total arsenic concentration should be in the approximate range of 10–100 mg/L to achieve this high adsorption density. Considering some extreme arsenic concentration conditions (Nordstrom and Alpers [27] reported an As concentration up to 850 mg/L in an iron mountain), a broader initial arsenic concentration range of 5–2000 mg/L was used. To

each of a series of 125 mL flasks containing 1 g adsorbent (dry weight), 100 mL As(V) solution containing 0.1 mol/L $NaNO_3$ as background electrolyte was added. The pH of the mixture was then adjusted using stock HNO_3 or NaOH solutions whose concentrations varied from 0.1 to 5 mol/L. All flasks were then sealed and shaken at 180 oscillation/min using an EBERBACH 6010 shaker for 24 h. The pH of the mixture was kept in the desired range by adjusting the pH periodically with stock HNO_3 or NaOH solutions. All of the adsorption runs were duplicated to ensure reproducibility. Mean values of the arsenate adsorbed versus equilibrium pH were plotted.

2.4. Chemical analyses

At the end of each adsorption run, the suspensions were filtered immediately through a 0.45-μm membrane filter made of cellulose acetate (MFS) and the filtrates were collected for the arsenate analyses. A graphite furnace atomic absorption spectrometer (AAnalyst 600, PerkinElmer Corp., Norwalk, CT, USA) with an instrumental detection limit (IDL) for arsenic of 0.3 μg/L was used to determine arsenic concentrations in solution. An Orion pH meter (perpHecT LoR model 370) with an Orion PerpHecT Triode pH electrode (model 9207BN) was used for pH measurements.

2.4.1. FTIR analyses

Diffuse reflectance FTIR spectra of powdered samples were recorded on a Nexus 470 FT-IR (Thermo Electron Corp.). The samples were diluted to a concentration of 2% with IR-grade KBr. Sixty-four signal-averaged scans were collected at 2 cm^{-1} resolution in the mid-IR region (4000–400 cm^{-1}) for pure KBr and for each KBr-mixed sample. Vibrational spectra of each sample were obtained by subtraction of the background spectra (pure KBr) from the spectra of KBr-mixed sample. The ATR-FTIR spectra of aqueous arsenate at various pH levels were examined using the attenuated total reflection Fourier transform infrared spectroscopy. The ATR cell was equipped with a trapezoidal ZnSe crystal (45° angle of incidence) as the internal reflection element. To minimize oxyanion reactions with the ZnSe crystal, the spectra were collected immediately after the solutions were transferred into the ATR cell. Background subtractions were made to remove bulk water spectra.

2.4.2. EXAFS analysis

Further structural analysis was performed via X-ray absorption spectroscopy using the X18B beamline at the national synchrotron light source (NSLS) at the Brookhaven National Laboratory to determine the As K-edge (11,867 eV) of the 0.100-M aqueous arsenate solutions exposed to GFH (obtained from the filtrates) at pH 7.4. The GFH was sealed between two layers of mylar foil held together by Kapton tape. $Na_2HAsO_4{\cdot}7H_2O$ (obtained from Alfa Aesar; 98+% purity) diluted in boron nitride was used as a reference standard. The transmission signal of Au foil (Au L_3-edge at 11,919 eV) was used as a reference to calibrate the energy positions along with the reference standard [28]. A double crystal Si(1 1 1) monochromator was used for energy selection and spectra were obtained in the fluorescence mode using a 13-element Ge detector. Ion chambers employed an 8:2 N_2-to-Ar gas mixture. Data were processed using the IFEFFIT library of numerical XAS algorithms written in Perl programming using the ab initio EXAFS code, FEFF 6.01 [29,30]. In order to fit the EXAFS data, distances from the absorber (As) to the first shell O atoms and second-shell As–Fe were determined by single-scattering theoretical phase shift and amplitude functions generated from FEFF 6.01 using atomic clusters generated from the crystal structure of scorodite ($FeAsO_4{\cdot}2H_2O$) [31].

3. Results and discussion

3.1. Characterization of GFH

The ζ-potentials of GFH were determined as a function of pH using 0.01 mol/L $NaNO_3$ as the supporting electrolyte, as demonstrated in Fig. 1(a). It was found that the isoelectric point (IEP) occurred at pH 8. The SEM image of GFH was shown in Fig. 1(b). GFH has very rough surface and large size. XRD analysis revealed that GFH is a ferric oxide hydroxide (akaganeite, FeOOH) (JCPDS 34-1266). The BET surface area of GFH is 206 m^2/g. In addition, GFH has very large pore volume (0.76 cm^3/g) and average pore size (14.8 nm).

3.2. Arsenate adsorption edges on GFH

Arsenate speciation is pH dependent and H_3AsO_4, $H_2AsO_4^-$, $HAsO_4^{2-}$ and AsO_4^{3-} are the dominant species in the following pH ranges: <2.3, 2.3–6.8, 6.8–11.3, and >11.3,

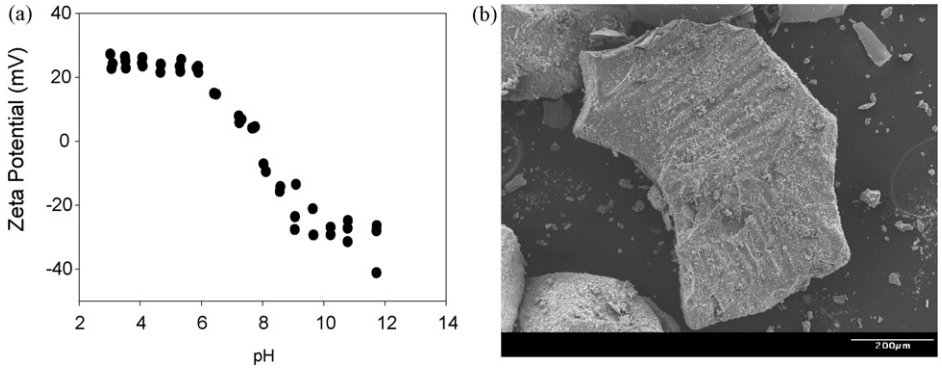

Fig. 1. (a) Zeta potential of GFH as a function of pH using 0.01 M $NaNO_3$ as the supporting electrolyte and (b) SEM image of GFH.

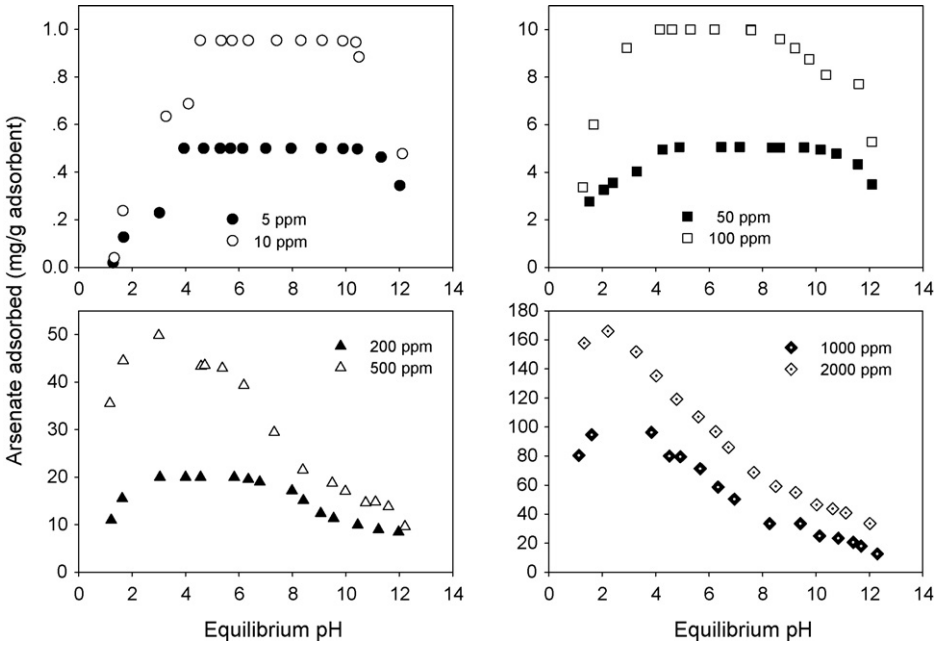

Fig. 2. Adsorption of arsenate on granular ferric hydroxide as functions of pH and concentration (concentration of granular ferric hydroxide, 10 g/L; arsenate concentration, 5–2000 ppm as As(V)).

respectively. In addition, the surface charge of GFH is pH dependent. At pH values below 8 (pH_{pzc} 8), the surface of GFH particles is positively charged and vice versa, which indicates that surface site speciation changes with pH. Consequently, the adsorption of arsenate on GFH is expected to depend on pH. The effect of pH on As(V) adsorption on GFH in the pH range of 1–13 at initial As(V) concentrations ranging from 5 to 1000 mg/L under 10 g/L sorbent conditions presented in Fig. 2. Arsenate adsorption behavior is strongly influenced by pH. When the initial arsenate concentration was no more than 200 mg/L, a broad adsorption maximum was observed. The broad adsorption maxima with more than 99% adsorption were observed at pH 4.0–10.4, 4.6–10.4, 4.9–10.0, 4.2–7.6 and pH 3.0–6.3 corresponding to the initial arsenate concentrations of 5, 10, 50, 100 and 200 mg/L, respectively. Distinct adsorption maxima were observed at pH 3.0, 2.7 and 2.2 for the initial arsenic concentrations of 500, 1000 and 2000 mg/L, respectively. Substantially less arsenate was adsorbed at pH values higher or lower than the pH at which the adsorption maxima appeared, which was associated the decrease of GFH surface charge with increasing pH and the variation of arsenic species with pH. Rau et al. [32] employed a high arsenate concentration of 1000 mg/L in their adsorption tests and reported that the arsenate adsorption maximum appeared at pH 1.8 on iron(III)-chelated iminodiacetate resins. The appearance of adsorption maxima at such low pH level indicated that the potential of GFH to be used in the removal of As(V) from acidic industrial effluents.

The adsorption maxima became narrower and the arsenate adsorption edge on GFH at alkaline pH end shifted to the low pH range with increasing initial arsenate concentration. Jia et al. [33] concluded that at basic pH arsenate was sorbed on ferrihydrite predominantly via surface adsorption. Therefore, the increase in competition from hydroxide ion reduced the arsenic adsorption as the pH was increased, and the gradual saturation of the adsorption sites under high arsenic loading conditions shifted the arsenate adsorption edge on GFH at alkaline pH end to the low pH range as the initial arsenate concentration was increased. This trend was also observed for As(V) adsorption on titanium dioxide [34] and on ferrihydrite [35] at various initial As(V) concentrations.

A very interesting phenomenon was observed in this study that the adsorption edge of arsenate on GFH at very acidic pH end shifted slightly to the high pH range at an initial arsenate concentration ranging from 5 to 50 mg/L but shifted to the low pH range as the initial arsenate concentration increased from 50 to 2000 mg/L. When the initial arsenic concentration was 5 or 10 mg/L, almost no arsenic was adsorbed at pH as low as 1.3. The fraction of adsorbed arsenic on GFH at same pH (below 2) increased as initial arsenic concentration increased. This phenomenon may be associated with the different reactions occurring at different initial arsenate concentrations. When the initial arsenate concentration is below 50 mg/L, arsenate was uptaken by GFH mainly by adsorption at acidic pH. Lowering pH facilitates the dissolution of GFH and the complexation of arsenate with ferric in solution and suppresses the adsorption of arsenate onto GFH. As surface precipitation is favored with increasing adsorbate concentration [36], arsenate may be adsorbed by GFH via both adsorption and precipitation when the initial arsenate concentration was increased. Jia et al. [33] observed surface precipitation of ferric arsenate on synthetic ferrihydrite at pH 3–5 when sorption density of As/Fe was between 0.125 and 0.49 and the arsenic equilibrium concentration was below 0.02–400 mg/L. Compared to two-dimensional surface complexation, the formation of ferric arsenate surface precipitate allows for the buildup of three-dimensional arsenate phase, thereby providing maximum arsenic removal.

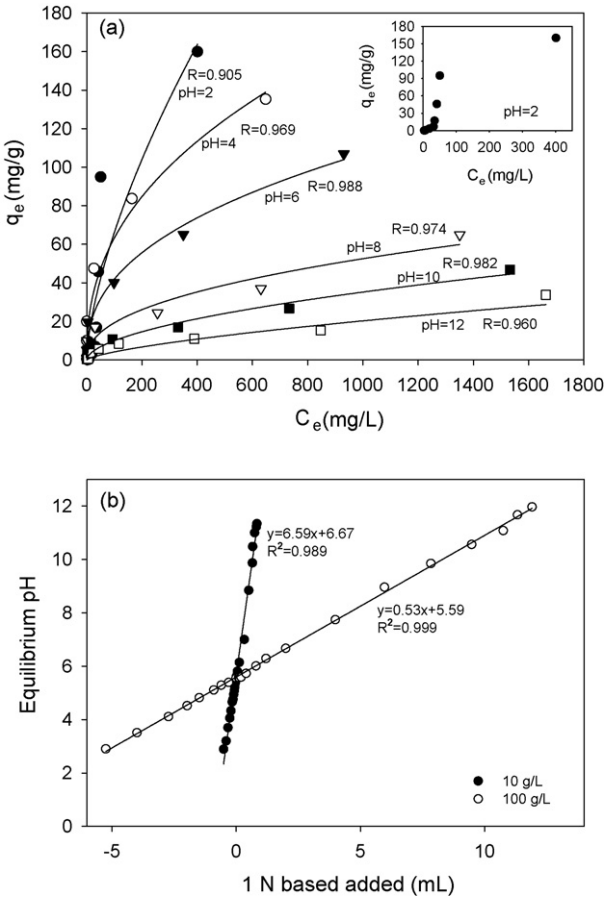

Fig. 3. (a) Adsorption isotherms of arsenate on GFH at various pH with the solid lines denote the simulation results based on the Freundlich equation (concentration of GFH, 10 g/L; initial arsenate concentration, 5–2000 mg/L as As(V)); (b) net titration curves of GFH at different sorbent concentrations.

3.3. Surface heterogeneity

Based on the adsorption data in Fig. 2, the arsenate adsorption isotherms, i.e. adsorption density as a function of equilibrium concentration for different pH conditions, were plotted, shown as points in Fig. 3(a). Results indicated that the adsorption density kept increasing with the increase of equilibrium arsenate concentration. Therefore, these isotherms were Freundlich type. The Freundlich equation was used to fit the data points:

$$q_e = K_F C_e^{1/n}$$

where q_e is the amount of solute adsorbed per unit weight of adsorbent (mg/g), C_e is the equilibrium concentration of solute in the bulk solution (mg/L), K_F is the constant indicative of the relative adsorption capacity of the adsorbent (mg/g), and $1/n$ is the constant indicative of the intensity of the adsorption. The solid lines in Fig. 3(a) are curve fitting results, with high R^2 values ($\geq$0.960) except at pH 2. It suggests that the GFH has very heterogeneous surface sites, and more surface sites are available when the equilibrium concentration is increased.

According to IUPAC classification the adsorption isotherm of arsenate at pH 2 shows a type-V adsorption pattern in the concentration range tested. The type-V adsorption isotherm is typical for adsorbent with mesoporous structures with the pore size in the range of 2–50 nm [37]. The adsorption starts on the pore surface following a type-III adsorption. When arsenate concentration increases, multilayer adsorption occurs until the whole pores are filled up. This result is consistent with the average pore size of 14.8 nm for GFH tested in this research. It suggests that the maximum adsorption of arsenate on GFH achieved at pH 2 was associated with the multilayer adsorption.

The acid–base titration was also performed to examine the surface acidity of GFH. Fig. 3(b) shows the net titration curves of GFH for two sorbent concentrations, 10 and 100 g/L. Results showed that both titration curves are straight lines without any inflexion points, which indicated that the GFH surface is very heterogeneous.

3.4. FTIR study of dissolved as species

The coordination chemistry of dissolved and adsorbed As species was investigated with ATR-FTIR and diffuse reflectance FTIR, respectively. The vibrational frequencies of the As–O group in solid phases containing arsenate species appears in the same positions as their counterparts observed under aqueous solution conditions (unattached to a solid) [38]. When protonated, the symmetry of AsO_4^{3-} is lowered from T_d to C_{3v}, C_{2v}, and C_{3v} in the formation of $HAsO_4^{2-}$, $H_2AsO_4^-$, and H_3AsO_4 [39], respectively, resulting in new bands. Fig. 4 demonstrates the ATR-FTIR spectra of a 0.1-mol/L sodium arsenate solution at pH 2.1, 4.2 and 8.9, respectively. The predominant species in sodium arsenate solution at pH 2.1 and 8.9 is a mixture of H_3AsO_4 and $H_2AsO_4^-$, $H_2AsO_4^-$, and $HAsO_4^{2-}$, respectively. A band at 859 cm^{-1} was observed for the spectrum of $HAsO_4^{2-}$ and assigned to ν_{as}(As–O) in $HAsO_4^{2-}$. Two peaks at 907 and 877 cm^{-1} were observed in the spectrum of $H_2AsO_4^-$ at pH 4.2 due to the splitting of the ν_3 mode. These two bands were assigned to ν_{as}(As–O) and ν_s(As–O), respectively. The ν_{as}(As–O) in $H_2AsO_4^-$ appearing at higher frequency than that in $HAsO_4^{2-}$ can be ascribed to the different modes of electron

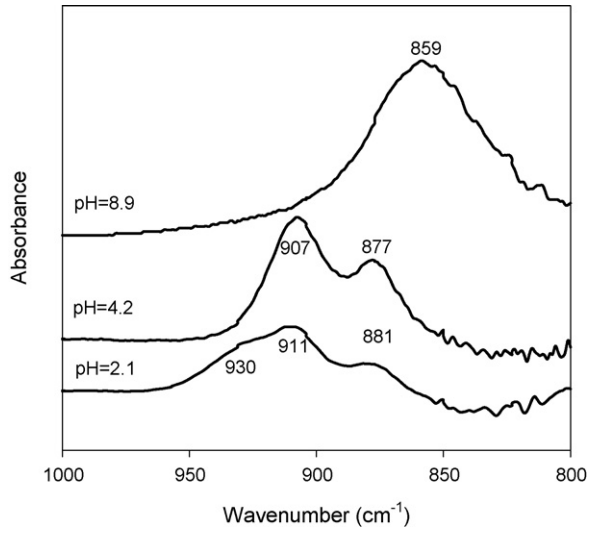

Fig. 4. ATR-FTIR spectra of 0.1 mol/L sodium arsenate solution at different pH.

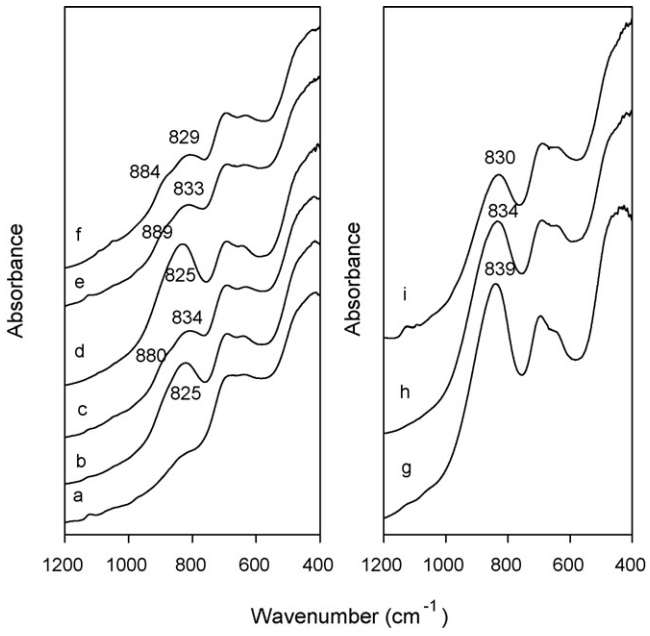

Fig. 5. Diffuse reflectance FTIR spectra of GFH under different pH and arsenic adsorption density (Γ) conditions: (a) GFH only; (b) pH 4.5, Γ = 80.3 mg As/g sorbent; (c) pH 6.3, Γ = 58.5 mg As/g sorbent; (d) pH 4.0, Γ = 135.0 mg As/g sorbent; (e) pH 6.3, Γ = 106.5 mg As/g sorbent; (f) pH 6.9, Γ = 69.8 mg As/g sorbent; (g) pH 1.3, Γ = 157.8 mg As/g sorbent; (h) pH 2.2, Γ = 166.0 mg/g; (i) pH 2.6, Γ = 160.8 mg As/g sorbent.

delocalization. Electron delocalization occurs on the two oxygen atoms in $H_2AsO_4^-$ and on the three oxygen atoms in $HAsO_4^{2-}$, which makes the bond order of the As–O bonds in these two moieties 3/2 and 4/3, respectively. At pH 2.1 a new band at 930 cm^{-1} appears, which we assign to theo the ν_{as}(As–O) stretch in H_3AsO_4.

3.5. FTIR study of adsorbed as species

The symmetry of arsenate was lowered when As was adsorbed onto GFH by forming inner-sphere complexes, leading to peak splitting or shifting. Fig. 5 shows the spectra of As(V) adsorbed onto GFH at various pH values and various adsorption densities, respectively. The peak positions of the adsorbed samples were significantly different from those of the dissolved As species, which we attributable to symmetry reduction arising from the oxyanion adsorption. If the symmetry reduction were caused by protonation, as would be the case for outer-sphere adsorption, the bands would exhibit at the similar positions as the corresponding dissolved As species. Therefore the band shift observed in this study indicated the formation of inner-sphere complexes. Due to the similarities of phosphate and arsenate sorption properties, the band assignments of adsorbed As(V) spectra are comparable to that of $(MO)_2PO_2$ surface complexes having C_{2v} symmetry [40–43]. Because metal ions are not as strongly coordinated to oxygen as protons [39–42], the O atom binding with Fe has an empty orbit that partially participates in electron delocalization and in turn the strength of the As–O bond is reduced. Therefore, the As–O bond in $(FeO)_2AsO_2$ would be weaker than that in $(HO)_2AsO_2^-$ and the As–O bond in $(FeO)AsO_3^-$ would be weaker than that in $(HO)AsO_3^{2-}$. Consequently, red-shifts in the IR stretch frequencies would be predicted as a result of arsenate complexation to GFH, which we observe (compare Fig. 4 with Fig. 5).

The spectra of arsenate adsorbed on GFH exhibited two bands at 880–889 and 825–839 cm^{-1}. However, the band at 880–889 cm^{-1} was only observed in the spectra at pH over 6 when $HAsO_4^{2-}$ began to appear in aqueous solution. The peak at 825–839 cm^{-1}, red-shifted relative to ν_{as}(As–O) in $HAsO_4^{2-}$ is assigned to ν(As–O) in the monodentate complex $(FeO)AsO_3^-$. The higher frequency band at 880–889 cm^{-1} is assigned to ν(As–O) in $(FeO)_2AsO_2$ complexes (bidentate complexes) as the frequency of this band is lower than ν(As–O) in $(HO)_2AsO_2^-$ and higher than that in $HAsO_4^{2-}$.

3.6. EXAFS analyses of arsenate coordination

EXAFS was used to further examine the local coordination environment (at pH 7.4) of the arsenate to the GFH to examine the modes of surface complexation. The contributions of three shells for GFH were used to account for the observed EXAFS oscillations. Fig. 6 shows the magnitude and real part of Fourier transformations (FTs) of the k^3-weighted As K-edge. The amplitudes of the FTs were phase corrected using scorodite to model the proposed structure. Interatomic distances in this figure have not been phase corrected; true distances to the next nearest neighbor atom can vary as much as 0.3–0.5 Å [44]. Table 1 lists the CN and σ^2 (with parameterization for σ^2 in parentheses) values used for the theoretical fits to the data as well as the calculated distances of As to the listed shells. One overall S_0^2 and ΔE_0 value were determined to fit the data. In fitting the GFH data, $S_0^2 = 0.197$ and $\Delta E_0 = 1.59$ were used to fit all of the paths (goodness of fit: $R = 0.0187$; $\chi^2_{red} = 48.2$). For data processing, a Hanning window and $R_{bkg} = 0.9$ was employed in all of the spectra. Radial distances determined from the fitting were determined in the k range (13 variables for 30 independent points; 2.0–10.0; 2.0–9.0 $Å^{-1}$) and the fit range (11 variables for 30 independent points; 1.0–6.0; 1.0–5.0) for GFH. As–Fe denotes single scattering paths while the As–O–O denotes a multiple scattering path. The multiple scattering path from As–O–O is from the absorbing As atom to an O atom and then to the opposite O atom aligned with that As atom and the first O atom. The value of 0.003 $Å^2$ was used as an initial guess estimate for the Debye–Waller factor, σ^2. The radial distances (R) from the absorber atom (As) to the three shells are summarized in Table 1.

The interatomic distance at ~1.65 Å (Table 1; Fig. 6) were indicative of a stable tetrahedral geometry for the arsenate coordinating to the GFH surfaces. This first shell distance has been widely observed for a variety media to which arse-

Table 1
Local coordination environment of arsenic on GFH

Shell	R (Å)	CN	σ^2 ($Å^2$)
As–O	1.650 ± 0.007	4	0.001 ± 0.002 (σ_1^2)
As–O–O	3.02 ± 0.02	6	0.0028 ± 0.0004 (2× (σ_1^2)
As–Fe	3.313 ± 0.006	2	0.001 ± 0.002 (σ_1^2)

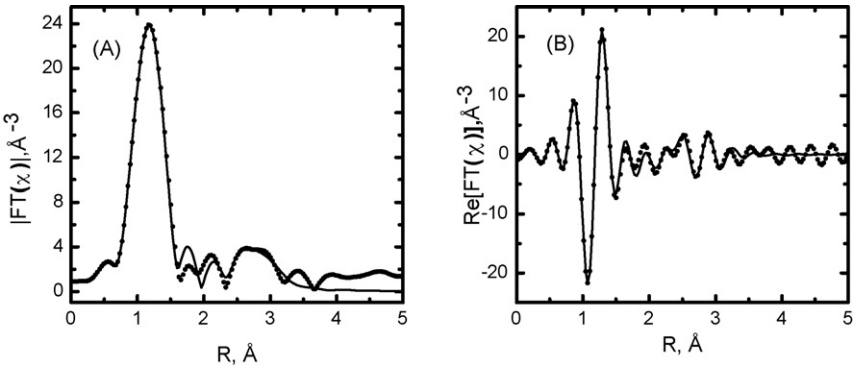

Fig. 6. The magnitude (A) and real part (B) of the Fourier transform of $\chi(k)\,k^3$-weighted data for GFH. The solid line denotes the theoretical fit and the filled circles denote the data. The peak positions are uncorrected for phase shifts.

nate coordinates [19,22,44–47]. The second peak position at ~3.02 Å is attributed to contributions from the multiple As–O–O scattering. The distance of 3.32 Å is in good agreement with previously published results for GFH (along with the first shell As–O distance), indicative of a bidentate binuclear coordination [19,22,46]. Since EXAFS analysis was performed with a sample collected at pH 7.4 (simulating natural ground water conditions) and the FTIR were performed with samples ranging from a pH of 1.3–6.9, the overall results showed that the formation of bidentate binuclear complexes between arsenate and GFH were favored at neutral pH while monodentate complexation is favored under acidic conditions.

In summary, the complexation of arsenate to GFH depends upon both pH and amount of loading of the oxyanion. Arsenate has a strong affinity for GFH and with monodentate complexation being highly favored at acidic pH while bidentate binuclear complexation dominates at neutral pH.

4. Conclusions

The adsorption envelopes of As(V) on GFH showed different shapes for different initial As(V) concentrations. Arsenate adsorption envelopes on GFH exhibited a broad adsorption maxima at sorbent concentration of 10 g/L when the initial As(V) concentration was less than 500 mg/L. However, when the initial As(V) concentration was further increased, distinct adsorption maxima appeared and shifted to lower pH. The adsorption isotherm of arsenate on GFH suggested that the GFH had very heterogeneous surface sites, and more surface sites were available when the equilibrium concentration was increased. Arsenate was adsorbed on GFH by forming complexes of two different structures, bidentate and monodentate, but it complexed with GFH forming only bidentate complexes at pH over 6, as revealed by the FTIR spectra. The EXAFS analyses confirmed that arsenate form bidentate binuclear complexes with GFH at pH 7.4 as evidenced by an average Fe-As(V) bond distance of 3.32 Å.

Acknowledgments

This work was partially supported by the Environmental Research Center (ERC) for emerging contaminants at the University of Missouri-Rolla (UMR). The authors thank Mr. Minghua Li at the University of Delaware for providing the zeta potential measurement. Conclusions and statements made in this paper are those of the authors, and in no way reflect the endorsement of the aforementioned funding party.

References

[1] V.K. Gupta, V.K. Saini, N. Jain, Adsorption of As(III) from aqueous solutions by iron oxide-coated sand, J. Colloid Interf. Sci. 288 (2005) 55–60.
[2] F.W. Pontius, K.G. Brown, C.J. Chen, Health implications of arsenic in drinking water, J. Am. Water Works Assoc. 86 (1994) 52–63.
[3] WHO, Guidelines for Drinking Water Quality. 1. Recommendations, World Health Organization, Geneva, 1993.
[4] USEPA, http://www.epa.gov/safewater/arsenic.html, 2004.
[5] M. Bissen, F.H. Frimmel, Arsenic—a review. Part II. Oxidation of arsenic and its removal in water treatment, Acta Hydrochim. Hydrobiol. 31 (2003) 97–107.
[6] M.R. Jekel, Removal of arsenic in drinking water treatment, in: J.O. Nriagu (Ed.), Arsenic in the Environment. Part I. Cycling and Characterization, John Wiley & Sons, New York, 1994, pp. 119–132.
[7] W.M. Mok, C.M. Wai, Mobilization of arsenic in contaminated river waters, in: C.M. Wai, J.O. Nriagu (Eds.), Arsenic in the Environment. Part I. Cycling and Characterization, John Wiley & Sons, New York, 1994, pp. 99–117.
[8] P.L. Smedley, D.G. Kinniburgh, A review of the source, behavior, and distribution of arsenic in natural waters, Appl. Geochem. 17 (2002) 517–568.
[9] J.F. Ferguson, J. Gavis, A review of the arsenic cycle in nature waters, Water Res. 6 (1972) 1259–1274.
[10] H.W. Chen, M.M. Frey, D. Clifford, L.S. McNeill, M. Edward, Arsenic treatment considerations, J. Am. Water Works Assoc. 91 (1991) 74–85.
[11] W. Driehaus, M. Jekel, U. Hildebrandt, Granular ferric hydroxide—a new adsorbent for the removal of arsenic from natural ferric hydroxide, J. Water SRT-Aqua 47 (1998) 30–35.
[12] G.L. Hatch, Meeting the new arsenic standard with a new iron based adsorbent media: POU applications, Water Cond. Purif. 44 (2002) 52–56.
[13] W.E. Halter, H.R. Pfeifer, Arsenic(V) adsorption onto α-Al_2O_3 between 25 and 70°C, Appl. Geochem. 16 (2001) 793–802.
[14] T.F. Lin, J.K. Wu, Adsorption of arsenite and arsenate within activated alumina grains: equilibrium and kinetics, Water Res. 35 (2001) 2049–2057.
[15] S. Goldberg, Competitive adsorption of arsenate and arsenite on oxides and clay minerals, Soil Sci. Soc. Am. J. 66 (2002) 413–421.
[16] X.J. Guo, F.H. Chen, Removal of arsenic by bead cellulose loaded with iron oxyhydroxide from groundwater, Environ. Sci. Technol. 39 (2005) 6808–6818.
[17] H. Genç, J.C. Tjell, D. McConchie, O. Schuiling, Adsorption of arsenate from water using neutralized red mud, J. Colloid Interf. Sci. 264 (2003) 327–334.

[18] G.A. Waychunas, J.A. Davis, C.C. Fuller, Geometry of sorbed arsenate on ferrihydrite and crystalline FeOOH—reevaluation of EXAFS results and topological factors in predicting sorbate geometry, and evidence for monodentate complexes, Geochim. Cosmochim. Acta 59 (1995) 3655–3661.
[19] G.A. Waychunas, B.A. Rea, C.C. Fuller, J.A. Davis, Surface-chemistry of ferrihydrite. 1. EXAFS studies of the geometry of coprecipitated and adsorbed arsenate. Geochim, Cosmochim. Acta 57 (1993) 2251–2269.
[20] T.H. Hsia, S.L. Lo, C.F. Lin, D.Y. Lee, Characterization of arsenate adsorption on hydrous iron-oxide using chemical and physical methods, Colloids Surf. A 85 (1994) 1–7.
[21] X.H. Sun, H.E. Doner, An investigation of arsenate and arsenite bonding structures on goethite by FTIR, Soil Sci. 161 (1996) 865–872.
[22] S. Fendorf, M.J. Eick, P. Grossl, D.L. Sparks, Arsenate and chromate retention mechanisms on goethite. 1. Surface structure, Environ. Sci. Technol. 31 (1997) 315–320.
[23] P.R. Grossl, M. Eick, D.L. Sparks, S. Goldberg, C.C. Ainsworth, Arsenate and chromate retention mechanisms on goethite. 2. Kinetic evaluation using a pressure-jump relaxation technique, Environ. Sci. Technol. 31 (1997) 321–326.
[24] P.R. Grossl, D.L. Sparks, Evaluation for contaminant ion adsorption–desorption on goethite using pressure-jump relaxation kinetics, Geoderma 67 (1995) 87–101.
[25] A. Jain, K.P. Raven, R.H. Loeppert, Arsenite and arsenate adsorption on ferrihydrite: surface charge reduction and net OH-release stoichiometry, Environ. Sci. Technol. 33 (1999) 1179–1184.
[26] U. Forstner, I. Haase, Geochemical demobilization of metallic pollutants in solid waste-implications for arsenic in waterworks sludges, J. Geochem. Explor. 62 (1998) 29–36.
[27] D.K. Nordstrom, C.N. Alpers, Negative pH, efflorescent mineralogy, and consequences for environmental restoration at the iron mountain superfund site, California, Proc. Natl. Acad. Sci. U.S.A. 96 (1999) 3455–3462.
[28] J.O. Cross, A.I. Frenkel, Use of scattered radiation for absolute X-ray energy calibration, Rev. Sci. Instrum. 70 (1990) 38–40.
[29] M. Newville, IFEFFIT: interactive XAFS analysis and FEFF fitting, J. Synchrotron Radiat. 8 (2001) 322–324.
[30] B. Ravel, M. Newville, ATHENA, ARTEMIS HEPHAESTUS: data analysis for X-ray absorption spectroscopy using IFEFFIT, J. Synchrotron Radiat. 12 (2005) 537–541.
[31] K. Kitahama, R. Kirayama, B. Yoshihisa, Refinement of the crystal structure of scorodite, Acta Crystallogr. B 31 (1975) 322–324.
[32] I. Rau, A. Gonzalo, M. Valiente, Arsenic(V) adsorption by immobilized iron mediation modeling of the adsorption process and influence of interfering anions, React. Funct. Polym. 54 (2003) 85–94.
[33] Y.F. Jia, L.Y. Xu, Z. Fang, G.P. Demopoulos, Observation of surface precipitation of arsenate on ferrihydrite, Environ. Sci. Technol. 40 (2006) 3248–3253.
[34] S. Bang, M. Patel, L. Lippincott, X.G. Meng, Removal of arsenic from groundwater by granular titanium dioxide adsorbent, Chemosphere 60 (2005) 389–397.
[35] K.P. Raven, A. Jain, R.H. Loeppert, Arsenite and arsenate adsorption on ferrihydrite: kinetics, equilibrium, and adsorption envelopes, Environ. Sci. Technol. 32 (1998) 344–349.
[36] D.A. Dzombak, F.M.M. Morel, Surface Complexation Modeling: Hydrous Ferric Oxide, John Wiley & Sons, New York, 1990.
[37] R.I. Masel, Principles of Adsorption and Reaction on Solid Surfaces, John Wiley & Sons, New York, 1996.
[38] S.C.B. Myneni, S.V. Traina, G.A. Waychunas, T.J. Logan, Vibrational spectroscopy of functional group chemistry and arsenate coordination in ettringite, Geochim. Cosmochim. Acta 62 (1998) 3499–3514.
[39] S.C.B. Myneni, S.V. Traina, G.A. Waychunas, T.J. Logan, Experimental and theoretical vibrational spectroscopic evaluation of arsenate coordination in aqueous solutions, solids, and at mineral–water interfaces, Geochim. Cosmochim. Acta 62 (1998) 3285–3300.
[40] M.I. Tejedor-Tejedor, M.A. Aderson, Protonation of phosphate on the surface of goethite as studied by CIR-FTIR and electrophoretic mobility, Langmuir 6 (1990) 602–613.
[41] W. Gong, A real time in situ ATR-FTIR spectroscopic study of linear phosphate adsorption on titania surfaces, Int. J. Miner. Process 63 (2001) 147–165.
[42] X.H. Guan, Q. Liu, G.H. Chen, C. Shang, Surface complexation of condensed phosphate to aluminum hydroxide: an ATR-FTIR spectroscopic investigation, J. Colloid Interf. Sci. 289 (2005) 319–327.
[43] M. Pena, X.G. Meng, G.P. Korfiatis, C.Y. Jing, Adsorption mechanism of arsenic on nanocrystalline titanium dioxide, Environ. Sci. Technol. 40 (2006) 1257–1262.
[44] C. Jing, S. Liu, M. Patel, X.G. Meng, Arsenic leachability in water treatment adsorbents, Environ. Sci. Technol. 39 (2005) 5481–5487.
[45] A.C.Q. Ladeira, V.S.T. Ciminelli, H.A. Duarte, M.C.M. Alves, A.Y. Ramos, Mechanism of anion retention from EXAFS and density functional calculations: arsenic(V) adsorbed on gibbsite, Geochim. Cosmochim. Acta 65 (2001) 1211–1217.
[46] D.M. Sherman, S.R. Randall, Surface complexation of arsenic(V) to iron(III) (hydr)oxides: structural mechanism from ab initio molecular geometries and EXAFS spectroscopy, Geochim. Cosmochim. Acta 67 (2003) 4223–4230.
[47] B.T. Beaulieu, K.S. Savage, Arsenate adsorption structures on aluminum oxide and phyllosilicate mineral surfaces in smelter-impacted soils, Environ. Sci. Technol. 39 (2005) 3571–3579.